Multidimensional Separation of Chiral Amino Acid Mixtures in a Multilayered Three-Dimensional Hybrid Microfluidic/Nanofluidic Device

ARTICLE *in* ANALYTICAL CHEMISTRY · MAY 2009

Impact Factor: 5.64 · DOI: 10.1021/ac802630p · Source: PubMed

7 AUTHORS, INCLUDING:

Bruce Flachsbart
University of Illinois, Urbana-Champaign
18 PUBLICATIONS **376** CITATIONS
SEE PROFILE

Jonathan Sweedler
University of Illinois, Urbana-Champaign
511 PUBLICATIONS **15,113** CITATIONS
SEE PROFILE

Published in final edited form as:
Anal Chem. 2009 April 1; 81(7): 2715–2722. doi:10.1021/ac802630p.

Multidimensional Separation of Chiral Amino Acid Mixtures in a Multilayered Three Dimensional Hybrid Microfluidic/Nanofluidic Device

Bo Young Kim[‡], **Jing Yang**, **Maojun Gong**[‡], **Bruce R. Flachsbart**[§], **Mark A. Shannon**[§], **Paul W. Bohn**[†], and **Jonathan V. Sweedler**[‡,*]

‡ *Department of Chemistry and Beckman Institute for Advanced Science and Technology, University of Illinois at Urbana-Champaign, Urbana, Illinois 61801*

§ *Department of Mechanical Science and Engineering, University of Illinois at Urbana-Champaign, Urbana, Illinois 61801*

† *Department of Chemical and Biomolecular Engineering and Department of Chemistry, University of Notre Dame, Notre Dame, Indiana 46556*

Abstract

Microscale total analysis systems (μTAS) allow high-throughput analyses by integrating multiple processes, parallelization and automation. Here we combine unit operations of μTAS to create a device that can perform multidimensional separations using a three-dimensional hybrid microfluidic/nanofluidic device composed of alternating layers of patterned polymethylmethacrylate and nanocapillary array membranes constructed from nuclear track-etched polycarbonate. Two consecutive electrophoretic separations are performed, the first being an achiral separation followed by a chiral separation of a selected analyte band. Separation conditions are optimized for a racemic mixture of fluorescein-labeled amino acids, serine and aspartic acid, chosen because there are endogenous D-forms of these amino acids in animals. The chiral separation is implemented using micellar electrokinetic chromatography using β–cyclodextrin as the chiral selector and sodium taurocholate as the micelle forming agent. Analyte separation is monitored by dual-beam laser-induced fluorescence detection. After separation in the first electrophoretic channel, the preselected analyte is sampled by the second-stage separation using an automated collection sequence with a zero-crossing algorithm for peak identification. The controlled fluidic environment inherent to the three-dimensional architecture enables a series of separations in varying fluidic environments and allows sample stacking via different background electrolyte pH conditions. The ability to interface sequential separations, selected analyte capture and other fluidic manipulations in the third dimension significantly improves the functionality of multilayer microfluidic devices.

*To whom correspondence should be addressed. Jonathan V. Sweedler, Phone: 217-244-4759, Fax: 217-265-6290, E-mail: jsweedle@illinois.edu.

Conflict of Interest Statement

The authors declare that there is no financial and/or commercial conflict of interest.

Supporting Information Available

Optical components and the schematic diagram of the custom-built, dual-beam laser-induced fluorescence detection system shown with a mounted microfluidic device on the instrument. This material is available free of charge via the Internet at http://pubs.acs.org.

Keywords

hybrid microfluidic/nanofluidic device; nanocapillary array membrane; automated microscale total analysis system; multidimensional separation; fraction collection

Introduction

Many questions arise when investigating biological systems that cannot be resolved with a single measurement technique. More often, a sequence of chemical and/or biochemical experiments are needed in order to attain unambiguous answers. Multistep analyses concomitantly require low limits of detection, efficient material transport and separation of analytes into pure fractions for further characterization. Microscale total analysis systems (μTAS)[1] have the ability to integrate a series of experiments on small platforms, thereby enabling complex analyses of mass- and volume-limited samples such as single cells or subcellular components. These approaches facilitate the investigation of dynamic intracellular events and/or intercellular signaling networks at the molecular level with temporal and spatial control.

Since the work of O'Farrell,[2] a multidimensional separation of protein using isoelectric focusing and sodium dodecyl sulfate polyacrylamide gel electrophoresis, multidimensional separations of complex biological samples have been carried out in various formats not only at conventional but also at miniaturized scales. Representative examples at the conventional scale of two- and three-[3] dimensional separations include tandem liquid chromatography,[4, 5] tandem capillary electrophoresis,[6–8] and combinations of these separation techniques.[9, 10] In addition, these approaches have been downscaled to miniaturized formats as well, such as multidimensional separations using planar microfabricated glass chips.[11–14] Here we present a two-dimensional separation using a microfabricated polymer chip using a heart-cutting approach[15] from the first dimension to the second dimension, although our system should be capable of performing a more comprehensive analyte transfer[3, 5, 9] by modulating the operation of the device.

Previously, we and others[16–26] have reported hybrid microfluidic/nanofluidic devices in two-dimensional (2D) or three-dimensional (3D) formats as possible functional components of μTAS. Adding nanofluidic elements, such as nanocapillary array membranes (NCAMs), to microfluidic systems introduces unique fluidic characteristics and functions (e.g., digital switching) to the microfluidic network. Some examples of the application of these hybrid devices include concentration,[27] rapid mixing,[24] size-selective transport,[22] ion selective transport,[28–31] and fluidic isolation.[18] The unique functional properties of the devices are due to the size of the nanofluidic channel dimension, a, being commensurate with the thickness of the Debye layer, κ^{-1}.[25] Thus, when the dimensionless group $\kappa \cdot a$ approaches unity, unique nanoscale flow properties emerge.

Here, we use a 3D polymethylmethacrylate (PMMA)-polycarbonate hybrid microfluidic/nanofluidic system[19] (Figure 1) as a multidimensional separation system with automated control[26] that meets the requirements of multifunctional μTAS. One advantage of this system is that the unit operations can be extended as needed while maintaining a compact size, allowing a series of analyses of complex real-world samples in one platform. To illustrate these capabilities, we present multidimensional separations of fluorescein isothiocyanate (FITC)-labeled racemic amino acid mixtures as a model system. The 2D separation is comprised of: (1) an initial achiral electrophoretic separation of amino acids; (2) collection of a specific band from this separation via an NCAM into a discrete, vertically-separated microchannel; and (3) a second chiral separation of the initially collected racemic mixture of labeled amino acids.

This system provides both a device and protocol for analyses and discovery of endogenous free D-amino acids. One application is for brain tissue analysis, which demands efficient mass- and volume-limited sample handling during multiple analytical steps.

As early as 1935, Krebs[32] reported D-amino acid oxidase (E. C. 1.4.3.3.) in mammalian liver and kidney, but the biochemical properties of this enzyme were not well studied because of the long-standing belief in homochirality[33]—that amino acids or peptides and proteins in higher-order organisms are exclusively composed of the L-form. However, advances in analytical techniques have enabled researchers to glean evidence for the existence of endogenous free D-amino acids, and D-amino acid-containing peptides and proteins, in a wide variety of animals such as mollusks[34–36] and mammals,[37] including humans.[33, 38, 39] Recent studies suggest that free endogenous D-amino acids, such as D-Ser[40, 41] and D-Asp,[34, 35, 42, 43] which are found in the central nervous system and peripheral tissues in significant amounts, have specific biological functions.[37, 44] Evidence obtained from D-amino acid-related studies suggests that D-Ser plays an important role as a neurotransmitter and D-Asp is involved in development and regulation of the endocrine system.[44]

To implement these studies, we created two distinct separations, one to resolve the amino acids and one for chiral discrimination. To achieve multidimensional separation, the first-stage is performed via capillary zone electrophoresis (CZE), a frequently used separation technique on microfluidic platforms.[45] This preference is due to the method's favorable scaling laws, ease of implementation, and because the plate count (*N*) can be independent of the capillary length.[46–48] The second-stage chiral separation is accomplished with cyclodextrin (CD)-modified micellar electrokinetic chromatography (MEKC),[49, 50] introduced by Terabe *et al.*[51–54] after their first demonstration of MEKC for separation of hydrophobic neutral compounds in CZE. While CZE separates analytes based on their charge and size (modified by interactions with the electrolyte), in MEKC, the micelles not only solvate hydrophobic molecules but also provide a pseudostationary phase. Therefore, analytes with the same mobility may partition differentially into micelles if they experience a differential chemical interaction with the micelle and thus become separated. CD, a cyclic oligosaccharide, is used as a chiral selector in CD-MEKC where the chiral compounds are resolved by forming reversible inclusion complexes with CD and these pseudodiastereomers are separated by MEKC.[55]

We develop and optimize the operating conditions of the 3D PMMA hybrid microfluidic/nanofluidic platform for high throughput small-scale analyses in order ultimately to target single cell or subcellular analyses. The capabilities of the system are presented by two steps of separation to achieve chiral separation of racemic mixtures of amino acids such as Asp[34–36] and Ser,[56, 57] both of which may be involved in cell-cell signaling.[33, 39, 41] The automated device operation sequence is realized by extending previous work by Tulock *et al.*[26] to allow selected bands of an initial (achiral) separation to be captured sequentially and injected into a subsequent (chiral) separation. Although microfluidic platforms made of polymers enable creative designs via rapid prototyping, chemical compatibility issues may present challenges and limit the applications. We address these concerns by using fairly complex buffer systems, which are necessary for 2D separation of our analyte mixtures in a 3D PMMA hybrid microfluidic/nanofluidic device.[19]

Materials and Methods

Materials and reagents

All of the materials and chemicals were used without further purification. The buffers and analyte solutions were prepared with deionized (DI) water from PURELAB Ultra system (18.2 MΩ·cm, ELGA LabWater; High Wycombe, UK). The ingredients for buffer preparation and amino acid standards were purchased form Sigma-Aldrich (St. Louis, MO) and Thermo Fisher

Scientific (Suwanee, GA). The enantiomerically pure amino acid standards used in the experiments have 99% or higher purity. Cetyltrimethylammonium bromide (CTAB, ≥ 99%), fluorescein 5-isothiocyanate (FITC, ≥ 97.5%), β-cyclodextrin (β-CD, ≥ 99%) and sodium taurocholate hydrate (STC, $[\alpha]_D^{20}$+22°, 97%) were acquired from Sigma-Aldrich.

Buffers and analyte mixture preparation

Borate buffers (20 mM, pH 10.0; 50 mM, pH 9.3; 20 mM, pH 9.3) used in the experiments were made by preparing a stock solution of 50 mM sodium tetraborate decahydrate ($Na_2B_4O_7{\cdot}10H_2O$; MW 381.37) in DI water. The pH of the diluted solutions was adjusted by adding small volumes of equimolar solutions of boric acid (H_3BO_3; MW 61.83) or sodium hydroxide (NaOH; MW 40.00) as needed. Phosphate buffers (20 mM, pH 8.0; 50 mM, pH 8.0) were prepared by mixing equimolar solutions of sodium phosphate dibasic heptahydrate ($Na_2HPO_4{\cdot}7H_2O$; MW 268.07) and sodium phosphate monobasic monohydrate ($NaH_2PO_4{\cdot}H_2O$; MW 137.99). For the 2D separation system, the running buffer was prepared by adding sufficient non-labeled L-Asp to produce a 1 mM solution in 50 mM borate buffer (pH 9.3), then adding MeOH to 20% (v/v). The second-stage separation buffer was prepared by adding 18 mM β-CD and 6 mM STC to the borate buffer.

To prepare the FITC-amino acids, sufficient non-labeled amino acid (L-Ser; D-Ser; L-Asp; D-Asp; D-Phenylalanine (D-Phe); D/L-Phenylalanine (D/L-Phe); L-Asparagine (L-Asn); Glycine (Gly)) solution was added to 20 mM borate buffer (pH 10.0) to yield 1 mM solutions. These were then mixed with 1 mM FITC solution in acetone at a 4:1 amino acid:FITC molar ratio. The mixtures were incubated in the dark, overnight at room temperature. The FITC-amino acids were stored at −20°C and used within 2 weeks. No significant degradation was observed in freshly diluted solutions. The typical concentration of the prepared stock solution was 200 μM, which was then diluted with running buffer for experiments.

Preparation and structure of the multidimensional separation device

The multilayered 3D PMMA hybrid microfluidic/nanofluidic system for multidimensional separation was custom prepared by the previously reported fabrication process.[19] The multidimensional separation device is composed of six layers, including four thin PMMA layers (20-μm thick; Figure 1A(b), (c), (e), (f)), one polycarbonate cap (1.5-mm thick; Figure 1A (a)) and one polycarbonate nuclear track-etched (PCTE) NCAM (10-μm thick; Figure 1A (d), 220 nm pore size; GE Osmonics; Minnetonka, MN). The rectangular microfluidic channels (100 μm wide × 20 μm (deep) were created on thin PMMA layers by lithographic patterning and reactive ion etching (RIE) using an oxygen/argon plasma (RIE, 600 W, Axic, Inc., Santa Clara, CA). The spatially separated, crossing microfluidic channels were connected by a vertically aligned 220-nm pore-diameter NCAM. All layers were assembled together by adhesive contact printing. Macroscopic reservoirs, cut from pipette tips, were attached using epoxy. This ensured that an equal volume of solution filled each reservoir (typically ~30 μL–50 μL) so as to minimize the influence of hydrodynamic pressure and the pH change of buffers while conducting experiments. Figure 1A illustrates the layered structure of the device, while Figure 1B shows a photograph (i) and schematic illustration with channel designations (ii) of an operational device. The analyte source channel (Figure 1B (ii)) is 13-mm long, the first-stage separation channel is 28 mm (the effective capillary length for separation is approximately 21 mm), and the second-stage separation channel is ~45 mm (the effective capillary length for separation is ~35 mm). The macroscopic reservoirs are numbered and keyed to the applied voltages as indicated in the tables throughout unless otherwise specified.

Instrumentation

Experiments were carried out on a custom-built, dual-beam laser-induced fluorescence (LIF) detection system equipped with a custom-built voltage control system. This system was described elsewhere.[22, 26] In brief, a continuous wave 488 nm (20 mW), frequency-doubled solid-state laser was used for fluorescence excitation (PC13589, Newport Spectra-Physics Lasers, Mountain View, CA) and two separate photon-counting photomultiplier tubes (PMT) (HC124, Hamamatsu Photonics, Bridgewater, NJ) were used for fluorescence detection. Each PMT was placed in light-tight housing made of Delrin® and equipped with 150-μm pinholes, long-pass emission filters and mechanical shutters. The optical components and the schematic diagram of the system are illustrated in Supporting Information, Figure S1. The laser power is attenuated by a neutral density filter, and then the beam is split by a 50/50 beam splitter to generate the dual detection capability. Each beam passes through a dichroic mirror and is focused through a 10× objective lens, one from the bottom and the other from the top of the microfluidic device. The diameter of the focused spot size is *ca.* 30 μm for each beam focused on the microfluidic channels.

To induce electrokinetic transport, voltages were applied by inserting 250-μm diameter platinum electrodes into each reservoir. The voltages were generated from six individual voltage sources (BERTAN 602C-30P, Spellman High Voltage Company, Hauppauge, NY) controlled by two sets of home-built, eight-switch voltage relay controllers. (**Safety Concerns:** the voltage sources have to be properly grounded and caution must be taken when working with high voltage sources.) Data collection and relay controls for voltage manipulations were controlled by data acquisition cards (PCI 6601 and PCI 6703) and customized software written using LabVIEW software (National Instruments Corporation, Austin, TX).

Results and Discussion

First-stage separation

Our first goal was to configure the PMMA/polycarbonate device operation for separations and to create protocols for reproducible separations. Previously, we demonstrated that reproducible gateable manipulations were possible with hybrid microfluidic/nanofluidic devices made of polydimethylsiloxane (PDMS)[16, 22, 23] or PMMA.[19, 20] Using the PMMA device delineated in Figure 1, reproducible injections of FITC-Asp are shown in Figure 2A, where the relative standard deviation of the peak intensities of 5–10 consecutive injections varied between 1.2 and 3.5% on a day-to-day basis. The LIF detection point was approximately 0.5 mm from the analyte injection point. The applied voltages used during injection and flow are as listed in the table in Figure 2C.

The FITC-amino acids were injected using their electrophoretic mobility. Before the injection, ~357 V/cm was applied for 80 s across the first-stage separation channel to stabilize the baseline; next, biased injection of FITC-Asp was achieved by applying 600 V to each reservoir of the first-stage separation (receiving) channel while ~308 V/cm was applied across the analyte source channel to supply analyte to the cross section for injection. After injection, the reservoirs of the analyte source channel were floated, while the injected FITC-Asp was transported along the first-stage separation channel (357 V/cm). Similar voltage configurations, with appropriate small adjustments, were used for analyte transport in other experiments.

The next step was to optimize the injection. Fa *et al.*[18] reported that microfluidic channels interconnected by NCAMs can maintain discrete fluidic environments when the NCAM pore diameter is smaller than 50 nm and the ionic strength of the solution is lower than 50 mM, behavior ascribed to Debye layer overlap within the NCAM nanopores. As the pore diameter

or ionic strength of the solution becomes larger, the Debye layer collapses below the pore diameter,[58] the structure enters the $\kappa a \gg 1$ regime, and electromigration-mediated ion transfer across the nanocapillary array increases. In this work a 220 nm pore diameter NCAM was used, which allowed analyte injection predominantly via electromigration across the NCAM; this pore-sized NCAM does not offer complete fluidic isolation between the layers. Therefore, buffered media with high buffer capacity and larger reservoirs were used to maintain a consistent pH during all manipulations.

Often in CZE, the quality of the separation is limited by the relative length of the injection band compared to the capillary length.[59] Short, highly concentrated analyte injection plugs can improve separation efficiency. An analyte plug can be focused to a narrow band by mismatching conductivity buffers (field-enhanced sample stacking,[60, 61] transient isotachophoresis[62]) or by using different pH combinations (dynamic pH junction)[63] or additives in the background electrolyte (sample sweeping)[64] to exploit different transport velocities of sample components in different physical regions of the separation medium; as a result, the injected sample is stacked in a narrow band before separation. The mechanisms and applications of these online sample concentration methods were reviewed recently by Simpson *et al*.[65] In the present application to 2D separations, we require narrow peaks to allow the automated peak collection algorithm to function optimally, and also prefer larger injection plugs to accommodate lower concentration samples. Factors that influence the formation of longer injection plugs include the duration of injection and non-optimized injection voltage configurations, as illustrated in Figure 3A. Under the conditions shown, analytes were injected in both directions in the separation channel (i.e., towards reservoirs V2 and V3), inducing additional band broadening. As an alternative, V2 can float while analytes are injected but this strategy decreases bandwidth, consequently reducing the amount of analyte injected. To enhance transport in the analyte source channel, CTAB was added at low concentration (μM range) to the buffer, which induced a positive charge on the device surface, thus reversing the electroosmotic flow direction.

Figure 3B, C shows a separation of five FITC-amino acids. The electropherograms were selected from five reproducible consecutive injections and separations. The peaks in the electropherograms (Figure 3B, C) were assigned as Asp (i), Gly (iii), Ser (iv), Asn (v), and Phe (vi), determined by individually spiking each analyte in the sample mixture. Under these conditions (pH 9.3), net migration of the FITC-amino acids is determined mainly by their charge and size. In Figure 3B, the analyte mixture in 20 mM of borate buffer (pH 9.3) containing 25 μM of CTAB (analyte source buffer) was injected into the first-stage separation channel (20 mM borate buffer, pH 9.3). To improve the peak shapes, 20 mM of phosphate buffer (pH 8.0) was used in the first-stage separation channel, while the analyte source buffer was unchanged (pH 9.3; Figure 3C). During injection, the high pH buffer (pH 9.3) and CTAB increases the analyte transport through the analyte source channel and across the NCAM into the first separation stage, where the analytes are introduced into the lower pH buffer (pH 8.0). This reduces the negative charge-density of the analytes and thus, their electrophoretic mobility. The effect on Asp is greater, because it has an additional charged carboxylate. Therefore, the analytes within the injection plug are transiently stacked at the front end of the plug. Then, when the mode is changed to separation, the chemically distinct mixture components begin to transit the first-stage channel at characteristic velocities, thus becoming separated. The peak shapes are significantly improved (especially for FITC-Asp). The calculated plate counts of peaks in Figure 3B are 166 and 1036 for (i) and (iii), respectively, and in Figure 3C, are 1024 and 1627 for (i) and (iii), respectively. Compared to the typical plate count in CZE (~200,000) these numbers are low; but comparing Figure 3B to C shows that a significant improvement can be achieved by carefully optimizing the buffer composition in different device regions. The efficiency of the separation can also be improved by modulating

the pH and conductivity of the background electrolyte, using additives, and increasing the applied voltage or channel length.

Chiral separation and 2D separation with automated peak collection

In order to perform CD-MEKC, β-CD was used as a chiral selector and STC as a micelle-forming surfactant. This system is based on previously published work by Lu *et al.*[66] where separation conditions were optimized by comparing the quality of the separations using CZE at conventional scale. Using either CD or chiral surfactants individually can achieve chiral selectivity, but when they are combined, the resolution is greatly improved. We carefully adjusted the amount of STC, β-CD and MeOH so that the separation condition was chemically compatible with the 3D PMMA/polycarbonate hybrid microfluidic/nanofluidic platform. Figure 4 shows chiral separation demonstrated using an equimolar mixture of FITC-D/L-Asp and FITC-D/L-Ser and a chiral buffer compatible with the multilayer system. The calculated plate counts for each peak are 1328, 1559, 987 and 959 for FITC-L-Asp, FITC-D-Asp, FITC-L-Ser and FITC-D-Ser, respectively. The resolution (R_s) between the Asp enantiomer peaks is 1.04, and the R_s between the Ser enantiomer peaks is 1.18.

Previously, we reported automated fraction collection using a simpler PDMS-based hybrid microfluidic/nanofluidic device using a zero-crossing algorithm.[26] Here, we extended the previous strategy to accomplish a two-part separation sequence. The data collected by LIF 1 not only monitors the first-stage separation, but also triggers the designated peak collection sequence and the second-stage separation, sequentially. LIF 0 monitors the second-stage chiral separation as shown in Figure 5D. Briefly, LIF 1 triggers the automated peak collection and the second-stage separation sequence by constantly creating a trace $g(f(x))$ given by,

$$g(f(x))=f(x_n) - f(x_{n-\Delta x}) \quad (1)$$

where $f(x_n)$ is the signal acquired at the nth time point. The function of $g(f(x))$ is created by subtracting its own preceding recorded value by Δx, ($f(x_{n-\Delta x})$) from the real time data value ($f(x_n)$) collected by LIF 1. The offset value, Δx, is defined with respect to a contiguous set of data points. Assuming the peaks have Gaussian shapes, the algorithm assigns a running total value of "0" when $g(f(x_n))\geq 0$, "1" when $g(f(x_n))<0$ and the algorithm recognizes a change in these values when zero-crossing occurs and triggers the next sequence of the device control program. In order to minimize false-positive and false-negative peak identification, the algorithm allows the modulation of Δx and the frequency of the peak rejection criterion. Therefore, Eq. 1 achieves a digitally smoothed differentiation of the time-dependent LIF signal. Also, by designating the length of the capillary and the distance between the collection gate and the LIF detection point, the program can calculate the migration rate of the analyte peak, thus identifying the proper delay time between peak recognition and application of the collection-mode biases.

Using this program, desired amino acids can be collected after electrophoretic separation in the first stage, and an individual peak can be subjected to chiral separation in the second stage. Here we demonstrate the separation of the racemic mixture of FITC-D/L-Asp and FITC-D/L-Ser. The electropherograms shown in Figures 4 and 5 have been low-pass filtered using a fast Fourier transform low-pass filter with a cut-off frequency of 1 Hz to reduce high frequency noise. Figure 5A shows the schematic diagram of the device used for the experiment, with asterisks indicating where the separations were monitored and controlled. Figure 5B is a table showing the voltage and time controls. The electropherograms shown in Figure 5C, D are the first-stage achiral separation of the mixture and the 2D separation, respectively. Recognition of the FITC-D/L-Asp mixture peak initiated the peak collection (FITC-D/L-Asp peak), and

the second-stage chiral separation was accomplished with the optimized conditions for the chiral separation identified in the previous experiment (Figure 4). As shown in Figure 5, CTAB was added to the running and chiral buffers (by mixing 1 mM CTAB in water with either running buffer or chiral buffer at the ratio of 25:975 (v/v)) because: (1) it helped adjust the control parameters by increasing the S/N, and (2) it prevented the backflow of chiral buffer to the running buffer channel by reversing the EOF direction towards to outlet. The latter feature was evident in that irreproducible electropherograms were obtained in the first-stage separation, when CTAB was not added. The plate counts acquired from the electropherograms were 351, 624, 1384 and 1300 for the FITC-D/L-Asp (Figure 5C), FITC-D/L-Ser (Figure 5C), FITC-L-Asp (Figure 5D) and FITC-D-Asp (Figure 5D), respectively. The peak resolution between FITC-D/L-Asp and FITC-D/L-Ser (Figure 5C) was 1.98, and between FITC-L-Asp and FITC-D-Asp (Figure 5D), it was 1.06. In Figure 5D, because the first-stage electropherogram was acquired prior to the collection region, a small shoulder on the left side of the FITC-D/L-Ser peak appears that is part of the FITC-D/L-Asp collected into the second-stage separation. This was verified by comparing the migration time of the analytes.

Concluding Remarks

These experiments establish one of the first demonstrations of multidimensional (2D) separations in a 3D hybrid microfluidic/nanofluidic device. Coupling the sequential electrophoretic (first-stage) and chiral (second-stage) separations depends critically on an automated peak collection/injection capability. Although the conceptual coupling accomplished here is completely general, the specific implementation is particularly useful for the electrophoretic-chiral sequential separations demonstrated. In the future we anticipate that several further refinements will enhance device performance and increase its utility. First, by optimizing the first-stage separation conditions, either by adjusting solution conditions or by increasing the length of the first-stage column, more complex samples can be assayed. Second, the addition of multiple second-stage separation channels will allow multiple racemic pairs to be separated in the second separation stage. Of course, one layer of the device could be altered to incorporate the serial-to-parallel conversion and separations as demonstrated by Jacobson's group.[67, 68] It is important to note that the 3D format demonstrated here has important advantages in separation capacity, because the subsequent separations can all be accomplished in vertically separated layers. In principle, since the layers occupy only ~30 μm in the vertical direction, a large number of second-stage separation modalities can be achieved. Finally, although enhanced peak collection strategies can be implemented, their potential will depend on a careful study of the relationship between R_s in the first-stage separation and transfer efficiency.

In addition to improving device operation, device fabrication can be improved as well. Although the current fabrication process allows creative designs not possible with strictly planar microfluidic formats, the particular combination of adhesives, PMMA and polycarbonate used limits the use of specific pH ranges and buffer additives. Understanding how to extend the range of solution conditions that can be employed is an important objective of ongoing research. In addition, differential heat dissipation between multiple polymer layers, coupled with significant heat generation, can lead to mismatched thermal expansion and, ultimately, to device failure. For example, using thermal modeling of a PMMA microfluidic separation chip, Zhu *et al.*[69] showed that heat dissipation does not keep up with heat generation and suggested using active heat dissipation measures. We are currently exploring adding these measures to our 3D device structures. One attractive possibility involves incorporating metallic NCAMs that can serve as electrical and electrochemical elements, while simultaneously improving the heat dissipation.[70] As these device fabrication details are optimized, the 3D hybrid nanofluidic/microfluidic multilayer device architecture utilized here will offer an increasingly flexible and powerful analysis platform.

Acknowledgements

This material is based upon work supported by the National Science Foundation under Award Nos. DMI-0328162 and CHE-04-00768, the Department of Energy under Award No. DE FG02 07ER15851, the Strategic Environmental Research and Development Program, and the National Institutes of Health under Award No. NS031609. B. Y. Kim thanks the Korea Science and Engineering Foundation Grant funded by the Korean government (M06-2003-000-10304-0).

References

1. Manz A, Graber N, Widmer HM. Sens Actuators B-Chem 1990;1:244–248.
2. O'Farrell PH. J Biol Chem 1975;250:4007–4021. [PubMed: 236308]
3. Moore AW Jr, Jorgenson JW. Anal Chem 1995;67:3456–3463. [PubMed: 8686894]
4. Holland LA, Jorgenson JW. Anal Chem 1995;67:3275–3283. [PubMed: 8686888]
5. Bushey MM, Jorgenson JW. Anal Chem 1990;62:161–167. [PubMed: 2310013]
6. Hu S, Michels DA, Fazal MA, Ratisoontorn C, Cunningham ML, Dovichi NJ. Anal Chem 2004;76:4044–4049. [PubMed: 15253641]
7. Harwood MM, Christians ES, Fazal MA, Dovichi NJ. J Chromatogr A 2006;1130:190–194. [PubMed: 16782116]
8. Fazal MA, Palmer VR, Dovichi NJ. J Chromatogr A 2006;1130:182–189. [PubMed: 16781720]
9. Larmann JP Jr, Lemmo AV, Moore AW Jr, Jorgenson JW. Electrophoresis 1993;14:439–447. [PubMed: 8354227]
10. Moore AW Jr, Larmann JP Jr, Lemmo AV, Jorgenson JW. Methods Enzymol 1996;270:401–419. [PubMed: 8803979]
11. Gottschlich N, Jacobson SC, Culbertson CT, Ramsey JM. Anal Chem 2001;73:2669–2674. [PubMed: 11403315]
12. Rocklin RD, Ramsey RS, Ramsey JM. Anal Chem 2000;72:5244–5249. [PubMed: 11080871]
13. Ramsey JD, Jacobson SC, Culbertson CT, Ramsey JM. Anal Chem 2003;75:3758–3764. [PubMed: 14572041]
14. Liu YM, Sweedler JV. Anal Chem 1996;68:3928–3933. [PubMed: 8916451]
15. Majors RE. J Chromatogr Sci 1980;18:393–486. [PubMed: 7451635]
16. Cannon DM, Kuo TC, Bohn PW, Sweedler JV. Anal Chem 2003;75:2224–2230. [PubMed: 12918959]
17. Chatterjee AN, Cannon DM, Gatimu EN, Sweedler JV, Aluru NR, Bohn PW. J Nanopart Res 2005;7:507–516.
18. Fa K, Tulock JJ, Sweedler JV, Bohn PW. J Am Chem Soc 2005;127:13928–13933. [PubMed: 16201814]
19. Flachsbart BR, Wong K, Iannacone JM, Abante EN, Vlach RL, Rauchfuss PA, Bohn PW, Sweedler JV, Shannon MA. Lab Chip 2006;6:667–674. [PubMed: 16652183]
20. Gong M, Kim BY, Flachsbart BR, Shannon MA, Bohn PW, Sweedler JV. IEEE Sens J 2008;8:601–607.
21. Ismagilov RF, Ng JM, Kenis PJ, Whitesides GM. Anal Chem 2001;73:5207–5213. [PubMed: 11721920]
22. Kuo TC, Cannon DM Jr, Chen Y, Tulock JJ, Shannon MA, Sweedler JV, Bohn PW. Anal Chem 2003;75:1861–1867. [PubMed: 12713044]
23. Kuo TC, Cannon DM, Shannon MA, Bohn PW, Sweedler JV. Sens Actuators A-Phys 2003;102:223–233.
24. Kuo TC, Kim HK, Cannon DM, Shannon MA, Sweedler JV, Bohn PW. Angew Chem Int Edit 2004;43:1862–1865.
25. Kuo TC, Sloan LA, Sweedler JV, Bohn PW. Langmuir 2001;17:6298–6303.
26. Tulock JJ, Shannon MA, Bohn PW, Sweedler JV. Anal Chem 2004;76:6419–6425. [PubMed: 15516136]
27. Wang YC, Stevens AL, Han J. Anal Chem 2005;77:4293–4299. [PubMed: 16013838]

28. Zhang Y, Timperman AT. Analyst 2003;128:537–542. [PubMed: 12866863]
29. Pu Q, Yun J, Temkin H, Liu S. Nano Lett 2004;4:1099–1103.
30. Plecis A, Schoch RB, Renaud P. Nano Lett 2005;5:1147–1155. [PubMed: 15943459]
31. Kim SJ, Wang YC, Lee JH, Jang H, Han J. Phys Rev Lett 2007;99:044501. [PubMed: 17678369]
32. Krebs HA. Biochem J 1935;29:1620–1644. [PubMed: 16745832]
33. Fujii N, Saito T. Chem Rec 2004;4:267–278. [PubMed: 15543607]
34. Miao H, Rubakhin SS, Scanlan CR, Wang LP, Sweedler JV. J Neurochem 2006;97:595–606. [PubMed: 16539650]
35. Miao H, Rubakhin SS, Sweedler JV. Anal Chem 2005;77:7190–7194. [PubMed: 16285665]
36. Miao H, Rubakhin SS, Sweedler JV. J Chromatogr A 2006;1106:56–60. [PubMed: 16199049]
37. Hashimoto A, Oka T. Prog Neurobiol 1997;52:325–353. [PubMed: 9247969]
38. Jilek A, Kreil G. Monatsh Chem 2008;139:1–5.
39. Yoshimura T, Esaki N. J Biosci Bioeng 2003;96:103–109. [PubMed: 16233494]
40. Martineau M, Baux G, Mothet JP. Trends Neurosci 2006;29:481–491. [PubMed: 16806506]
41. Snyder SH, Kim PM. Neurochem Res 2000;25:553–560. [PubMed: 10905615]
42. Sakai K, Homma H, Lee JA, Fukushima T, Santa T, Tashiro K, Iwatsubo T, Imai K. Brain Res 1998;808:65–71. [PubMed: 9795139]
43. Wolosker H, D'Aniello A, Snyder SH. Neuroscience 2000;100:183–189. [PubMed: 10996468]
44. Fuchs SA, Berger R, Klomp LWJ, de Koning TJ. Mol Genet Metab 2005;85:168–180. [PubMed: 15979028]
45. Wu DP, Qin JH, Lin BC. J Chromatogr A 2008;1184:542–559. [PubMed: 18207148]
46. Ewing AG, Wallingford RA, Olefirowicz TM. Anal Chem 1989;61:A292–A303.
47. Jorgenson JW. Anal Chem 1986;58:A743–A760.
48. Jorgenson, JW. Methods: A Companion to Methods in Enzymology. Vol. 4. Academic Press; San Diego: 1992. p. 179-190.
49. Nishi H, Fukuyama T, Terabe S. J Chromatogr 1991;553:503–516.
50. Terabe S, Miyashita Y, Shibata O, Barnhart ER, Alexander LR, Patterson DG, Karger BL, Hosoya K, Tanaka N. J Chromatogr 1990;516:23–31.
51. Otsuka K, Terabe S, Ando T. J Chromatogr 1985;348:39–47.
52. Otsuka K, Terabe S, Ando T. J Chromatogr 1985;332:219–226.
53. Terabe S, Otsuka K, Ando T. Anal Chem 1985;57:834–841.
54. Terabe S, Otsuka K, Ichikawa K, Tsuchiya A, Ando T. Anal Chem 1984;56:111–113.
55. Vespalec R, Bocek P. Chem Rev 2000;100:3715–3754. [PubMed: 11749326]
56. Mothet JP, Parent AT, Wolosker H, Brady RO, Linden DJ, Ferris CD, Rogawski MA, Snyder SH. Proc Natl Acad Sci U S A 2000;97:4926–4931. [PubMed: 10781100]
57. Wolosker H, Sheth KN, Takahashi M, Mothet JP, Brady RO, Ferris CD, Snyder SH. Proc Natl Acad Sci U S A 1999;96:721–725. [PubMed: 9892700]
58. Kemery PJ, Steehler JK, Bohn PW. Langmuir 1998;14:2884–2889.
59. Huang XH, Coleman WF, Zare RN. J Chromatogr 1989;480:95–110.
60. Burgi DS, Chien RL. Anal Biochem 1992;202:306–309. [PubMed: 1519757]
61. Burgi DS, Chien RL. Methods Mol Biol 1996;52:211–226. [PubMed: 8746689]
62. Nishi H, Terabe S. J Chromatogr A 1995;694:245–276.
63. Britz-McKibbin P, Ichihashi T, Tsubota K, Chen DDY, Terabe S. J Chromatogr A 2003;1013:65–76. [PubMed: 14604109]
64. Quirino JP, Kim JB, Terabe S. J Chromatogr A 2002;965:357–373. [PubMed: 12236536]
65. Simpson SL Jr, Quirino JP, Terabe S. J Chromatogr A 2008;1184:504–541. [PubMed: 18035364]
66. Lu XN, Chen Y. J Chromatogr A 2002;955:133–140. [PubMed: 12061559]
67. Amarie D, Glazier JA, Jacobson SC. Anal Chem 2007;79:9471–9477. [PubMed: 17999467]
68. Lerch MA, Jacobson SC. Anal Chem 2007;79:7485–7491. [PubMed: 17718538]

69. Zhu, Y.; Bui, A. NSTI Nanotech 2006, NSTI Nanotechnology Conference and Trade Show; Boston, MA, United States. 2006. p. 655-658.

70. Piruska A, Branagan S, Cropek DM, Sweedler JV, Bohn PW. Lab Chip 2008;8:1625–1631. [PubMed: 18813383]

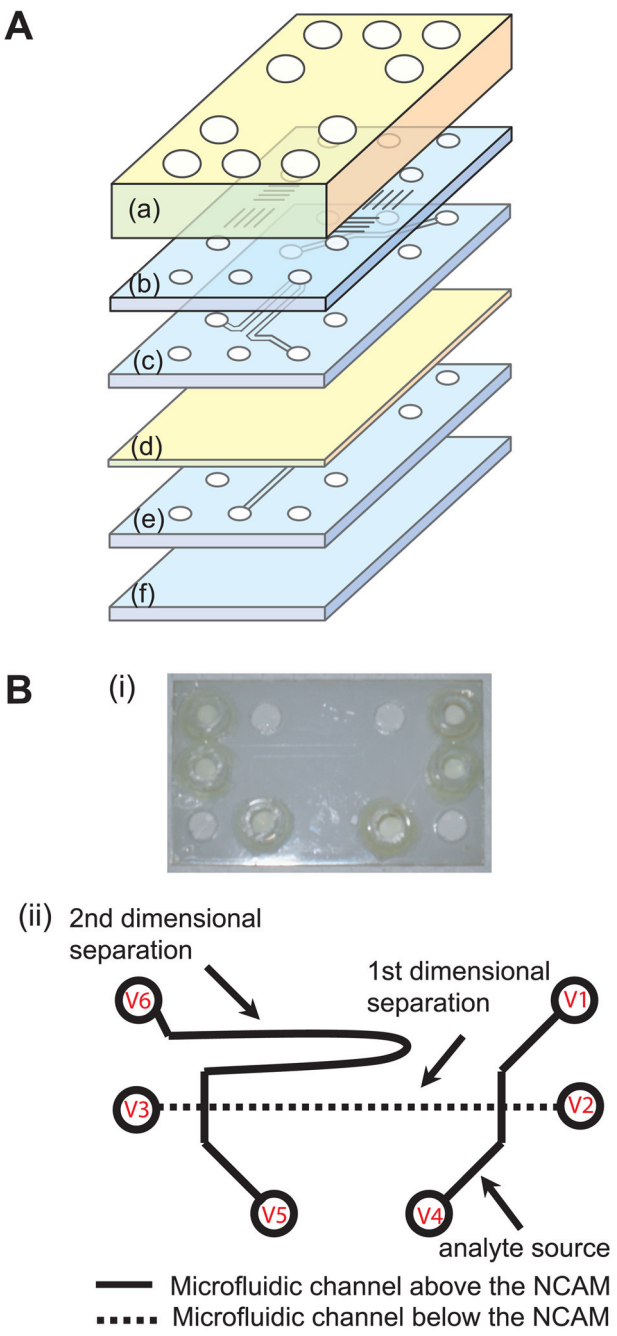

Figure 1. Schematic illustration of the device structure and photograph

(A) Describes the individual layers of the multilayered device; (a) is the 1.5-mm thick polycarbonate cap; (b), (c), (e) (patterned, 100 μm (width) × 20 μm (depth)) and (f) are 20-μm thick PMMA layers and (d) is a 10-μm thick NCAM. (B) Photo of a typical device (i) and a schematic diagram showing the microfluidic channel labeling scheme. (ii). NCAM is omitted in (B) (ii) for clarity.

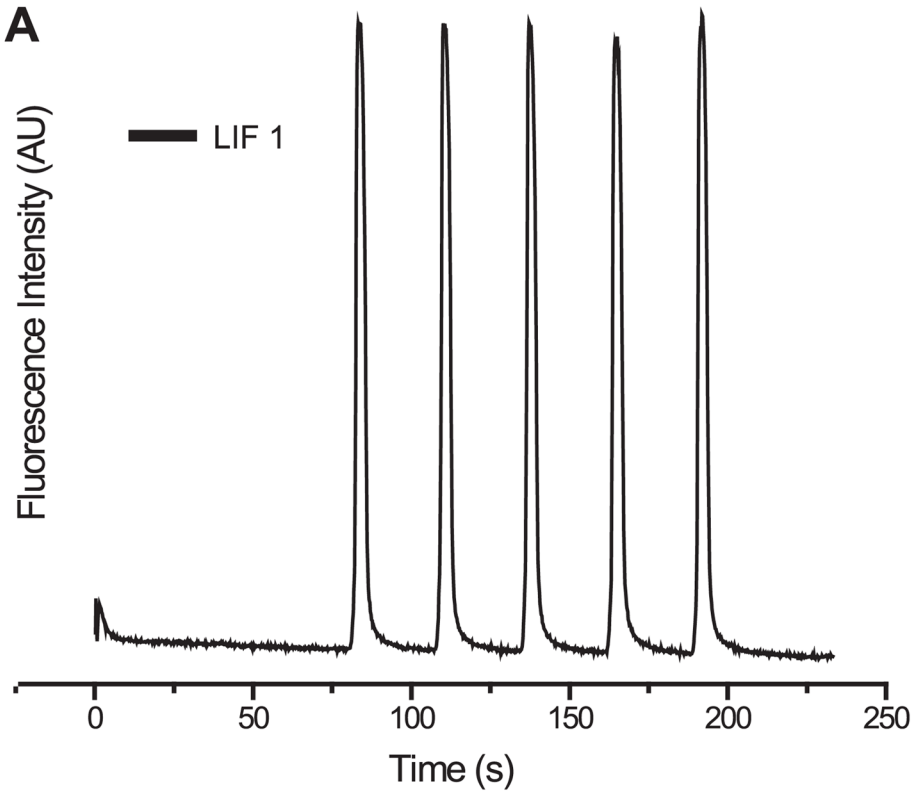

B

Voltage (V) \ Time (s)	Flow	Injection	Flow
	80	2	30 last flow 40
V1	F	G	F
V2	G	600	G
V3	1000	600	1000
V4	F	400	F
V5	F	F	F
V6	F	F	F

Figure 2.
Reproducible analyte injections. (A) LIF data from five consecutive sets of injection and flow of FITC-Asp from the analyte source channel to the first-stage separation channel. (B) Table illustrating the voltage manipulation scheme for operating the device during injections from the analyte source channel and subsequent first-stage separation (F: Floating; G: Grounded).

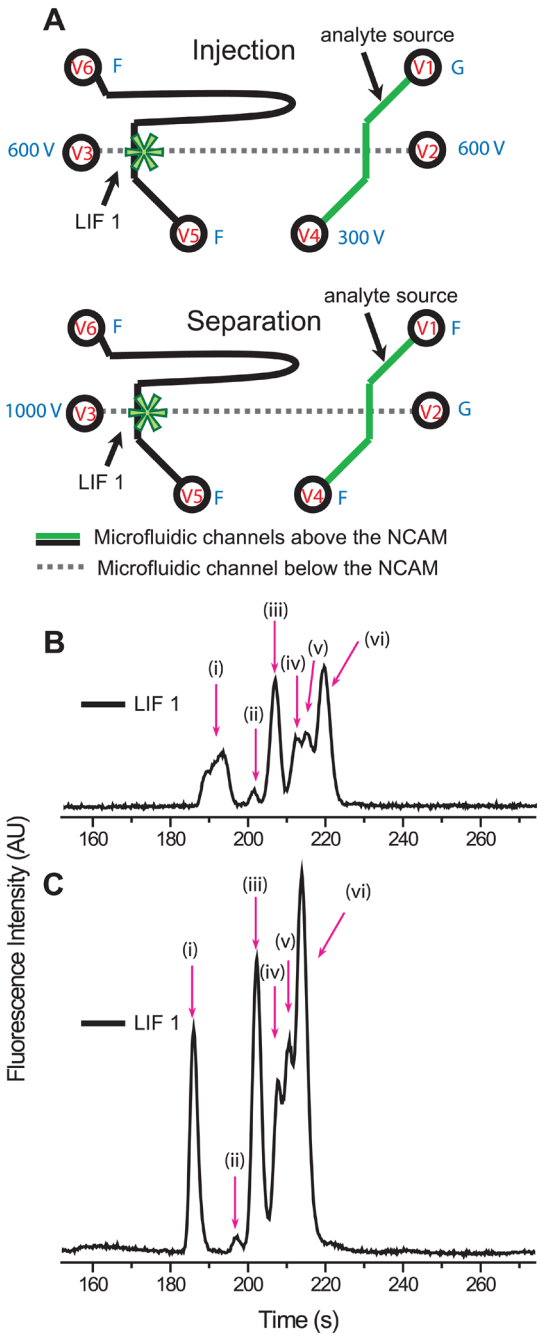

Figure 3.

The effect of a discrete buffered fluidic environment on separations. (A) Device operation scheme. (B) and (C) Electropherograms of FITC-amino acid mixtures (y-axis has arbitrary intensity values so that the intensity of (B) and (C) cannot be directly compared). The electropherograms were selected from five consecutive sets of injection and separation. The FITC-amino acid mixture was prepared in 20 mM borate buffer (pH 9.3) containing 25 μM of CTAB for both (B) and (C). The separation buffers were 20 mM borate buffer (pH 9.3) for experiment (B) and 20 mM phosphate buffer (pH 8.0) for experiment (C). (i), (ii), (iii), (iv), (v), and (vi) are FITC-Asp, unknown impurity, FITC-Gly, FITC-Ser, FITC-Asn, and FITC-Phe, respectively.

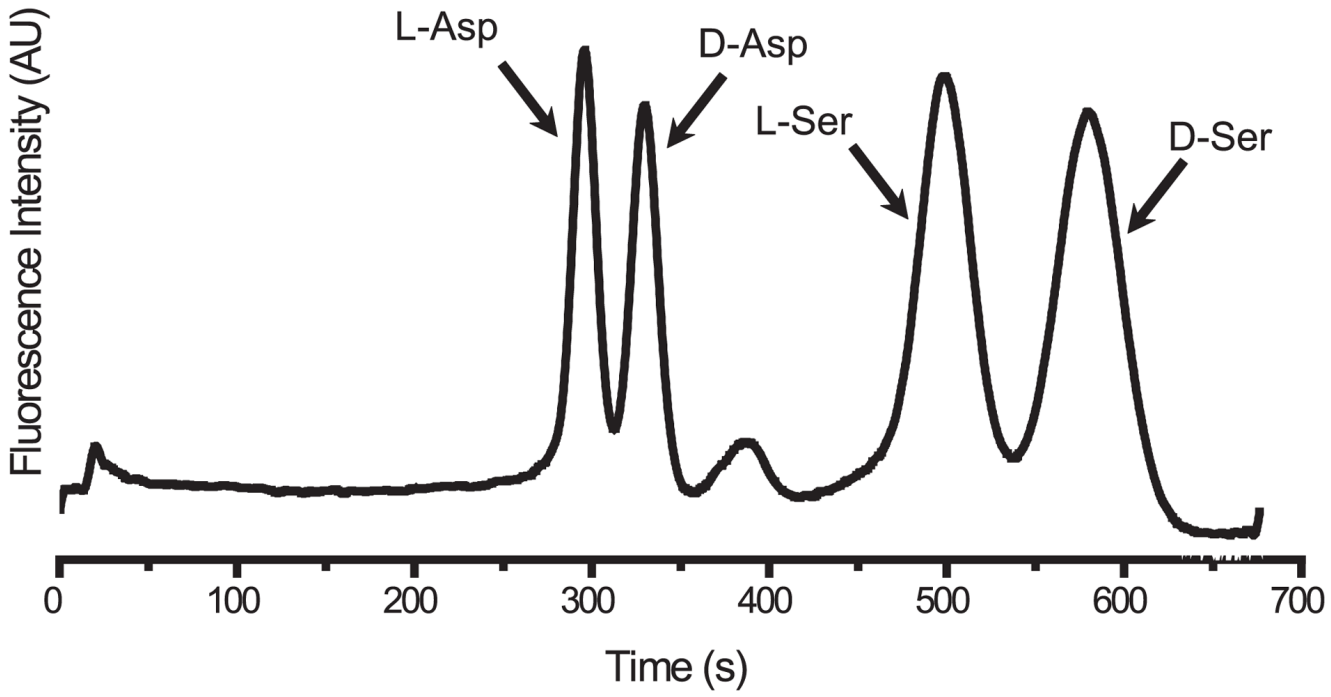

Figure 4.
Chiral separation demonstrated on a 3D PMMA microfluidic/nanofluidic device. The analyte was injected for 2 s. The LIF detection point was approximately 22 mm apart from the injection point. The analyte in the analyte source channel contained 10 μM of FITC-D/L-Asp and FITC-D/L-Ser in running buffer and the chiral separation was performed in chiral buffer.

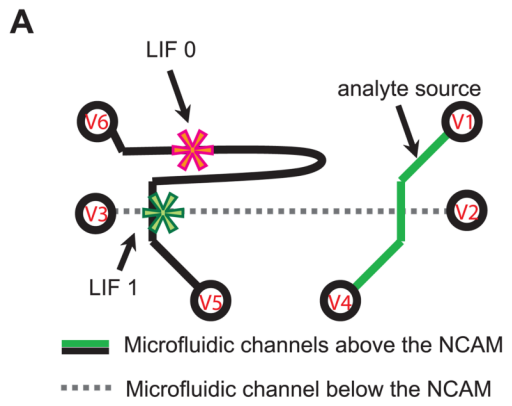

B

Time (s) / Voltage (V)	Injection	1st Separation	Collection	2nd Separation
	5		Asp 3	
V1	G	F	F	F
V2	600	G	G	F
V3	600	900	G	F
V4	400	F	F	F
V5	F	F	600	G
V6	F	F	800	900

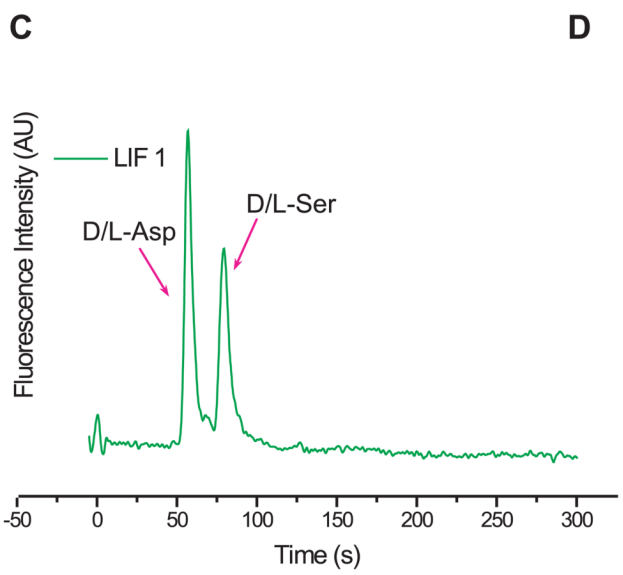

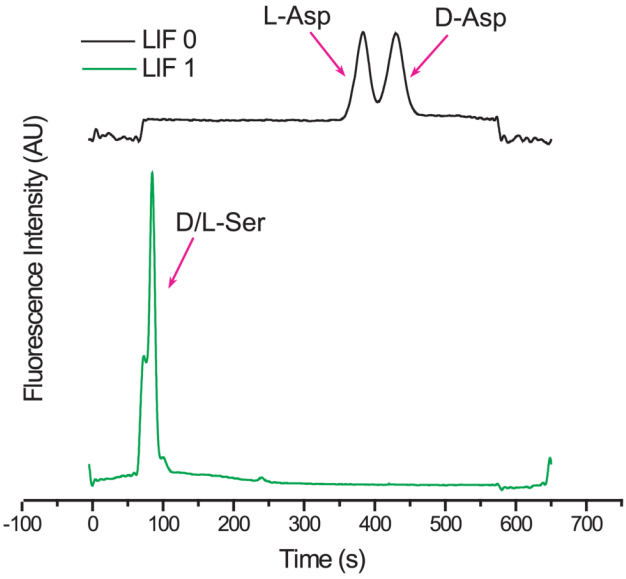

Figure 5.

Two-dimensional separation of FITC-amino acid mixture. (A) Layout of microfluidic channels and the voltage source connections on each reservoir. Asterisks indicate the focused excitation/data collection locations for each separation channel. LIF 1 and LIF 0 monitor the first (electrophoretic)- and second (chiral)-stage separations, respectively. (B) Table showing applied voltages during each phase of the sequential separations. (C) First-dimensional separation of a racemic mixture of fluorescein-labeled aspartic acid and serine. (D) The coupled two-stage separation of FITC-Asp and FITC-Ser, where the FITC-Asp is selectively transferred to the second-stage separation channel for the chiral separation. The peak shoulder of the D/L-Ser peak is part of the D/L-Asp peak, recognized and collected for the second-stage chiral separation.